

RESEARCH ARTICLE

Design of a novel multi-epitope vaccine candidate against hepatitis C virus using structural and nonstructural proteins: An immunoinformatics approach

Esmail Behmard¹, Hussein T. Abdulabbas², Saade Abdalkareem Jasim³, Sohrab Najafipour¹, Abdolmajid Ghasemian^{4*}, Akbar Farjadfar⁵, Ebrahim Barzegari⁶, Amin Kouhpayeh^{7*}, Parviz Abdolmaleki^{8*}

1 School of Advanced Technologies in Medicine, Fasa University of Medical Sciences, Fasa, Iran, **2** Department of Medical Laboratory Techniques, Faculty of Health and Medical Techniques, Imam Ja'afar Al-Sadiq University, Al Muthanna, Iraq, **3** Medical Laboratory Techniques Department, Al-maarif University College, Ramadi, Iraq, **4** Noncommunicable Diseases Research Center, Fasa University of Medical Sciences, Fasa, Iran, **5** Department of Medical Biotechnology, Fasa University of Medical Sciences, Fasa, Iran, **6** Medical Biology Research Center, Health Technology Institute, Kermanshah University of Medical Sciences, Kermanshah, Iran, **7** Department of Pharmacology, Fasa University of Medical Sciences, Fasa, Iran, **8** Department of Biophysics, Faculty of Biological Sciences, Tarbiat Modares University, Tehran, Iran

* parviz@modares.ac.ir (PA); kouhpayeha@gmail.com (AK); majidghasemian86@gmail.com (AG)



OPEN ACCESS

Citation: Behmard E, Abdulabbas HT, Abdalkareem Jasim S, Najafipour S, Ghasemian A, Farjadfar A, et al. (2022) Design of a novel multi-epitope vaccine candidate against hepatitis C virus using structural and nonstructural proteins: An immunoinformatics approach. PLoS ONE 17(8): e0272582. <https://doi.org/10.1371/journal.pone.0272582>

Editor: Manas Ranjan Dikhit, Rajendra Memorial Research Institute of Medical Sciences, INDIA

Received: February 10, 2022

Accepted: July 21, 2022

Published: August 30, 2022

Copyright: © 2022 Behmard et al. This is an open access article distributed under the terms of the [Creative Commons Attribution License](https://creativecommons.org/licenses/by/4.0/), which permits unrestricted use, distribution, and reproduction in any medium, provided the original author and source are credited.

Data Availability Statement: All relevant data are within the article and its [Supporting Information](#) files.

Funding: The authors received no specific funding for this work.

Competing interests: The authors have declared that no competing interests exist.

Abstract

Hepatitis C virus (HCV) infects the liver and causes chronic infection. Several mutations in the viral genome have been associated with drug resistance development. Currently, there is no approved vaccine against the HCV. The employment of computational biology is the primary and crucial step for vaccine design or antiviral therapy which can substantially reduce the duration and cost of studies. Therefore, in this study, we designed a multi-epitope vaccine using various immunoinformatics tools to elicit the efficient human immune responses against the HCV. Initially, various potential (antigenic, immunogenic, non-toxic and non-allergenic) epitope segments were extracted from viral structural and non-structural protein sequences using multiple screening methods. The selected epitopes were linked to each other properly. Then, toll-like receptors (TLRs) 3 and 4 agonists (50S ribosomal protein L7/L12 and human β -defensin 2, respectively) were added to the N-terminus of the final vaccine sequence to increase its immunogenicity. The 3D structure of the vaccine was modeled. Molecular dynamics simulations studies verified the high stability of final free vaccines and in complex with TLR3 and TLR4. These constructs were also antigenic, non-allergenic, nontoxic and immunogenic. Although the designed vaccine traits were promising as a potential candidate against the HCV infection, experimental studies and clinical trials are required to verify the protective traits and safety of the designed vaccine.

1. Introduction

Hepatitis C virus (HCV) is one of the most important human infectious diseases threatening the life of a large part of the international community [1–3]. The World Health Organization (WHO) has estimated that ~200 million cases are infected with the HCV worldwide, and 3–4 million new cases are diagnosed each year [4–6]. Liver cirrhosis and carcinoma are major consequences of chronic HCV infection. The treatment efficacy is insufficient due to various side effects of anti-HCV drugs and the development of drug resistance by the virus [7–10]. Therefore, there is an unmet requirement to develop new strategies such as vaccine design to reduce the HCV incidence and related mortality.

It is well known that a successful vaccination should be associated with sufficient immunity (through elicitation of immune responses) and protection [11, 12]. Various vaccine candidates have been developed against the HCV [13–15]. The design of a multi-epitope vaccine derived from the structural and non-structural protein sequences is promising and preferable than whole cell or inactivated candidates against viral pathogens [16–20]. These proteins play a major role in the process of viral penetration and replication within the host cell [9, 10]. Multi-epitope vaccines advantages over the inactivated or whole protein vaccines include lower costs and rapidity of production, higher immunity and safety potential, lower non-specific reactions or cross-reactivity and convenient manipulation [21–23]. Identification of potential epitopes capable of eliciting immune responses have become a challenge in current safety research [17, 18]. Application of basic structure design techniques and immunoinformatics tools in hybrid with dynamic mechanistic studies are promising to profoundly understand these mechanisms [16–18]. Among these methods, computational techniques draw attentions increasingly, because of their contribution to remarkable reduction of time and costs of vaccine design [14–20, 24]. With the advent of sequencing technologies, sufficient genomic and proteomic information have been provided from various viruses. As a result, peptide-based and epitope-based vaccines can be designed with the help of various bioinformatics tools [14–20, 24]. The design of epitope-based vaccines is now a familiar concept. Epitope-based vaccines against *Leishmania donovani* complex [15], Theileria parasites [16], Chikungunya virus [17], Human Herpes virus [18], human immunodeficiency virus (HIV) [19], Ebola virus [20], and human coronavirus [22] have been suggested to date. For successful development of peptide-based vaccines understanding the molecular details of antigen detection is an important and effective step. Though the identification of immunogenic epitopes has been facilitated by various algorithms, more computational studies are needed to prove the tendency and detail of interactions between the immune receptor and epitopes. Considering this, docking and molecular dynamics simulation services are effective sources of molecular-level structural information in immunology. Various Toll-like receptors (TLRs) such as TLR2, TLR3, TLR4 and TLR6 act as receptors of the viral proteins [25]. The membrane TLR4 and intracellular TLR3 agonist/adjuvant has been adopted for ligand and receptor interaction assessment in some studies of multi-epitope vaccine design [21, 22]. TLR3 plays a crucial role in the antiviral induction of hepatic macrophages and Kupffer cells via nuclear factor kappa B (NF- κ B) pathway and pro-inflammatory cytokines CXCL10. TLR4 agonist also provokes substantial immune responses [26].

In this study, a multi-epitope vaccine was designed against the HCV using immunoinformatics and computational methods from sequences of HCV structural and non-structural proteins.

2. Materials and methods

The basic steps of designing a multi-epitope vaccine are shown in the Fig 1.

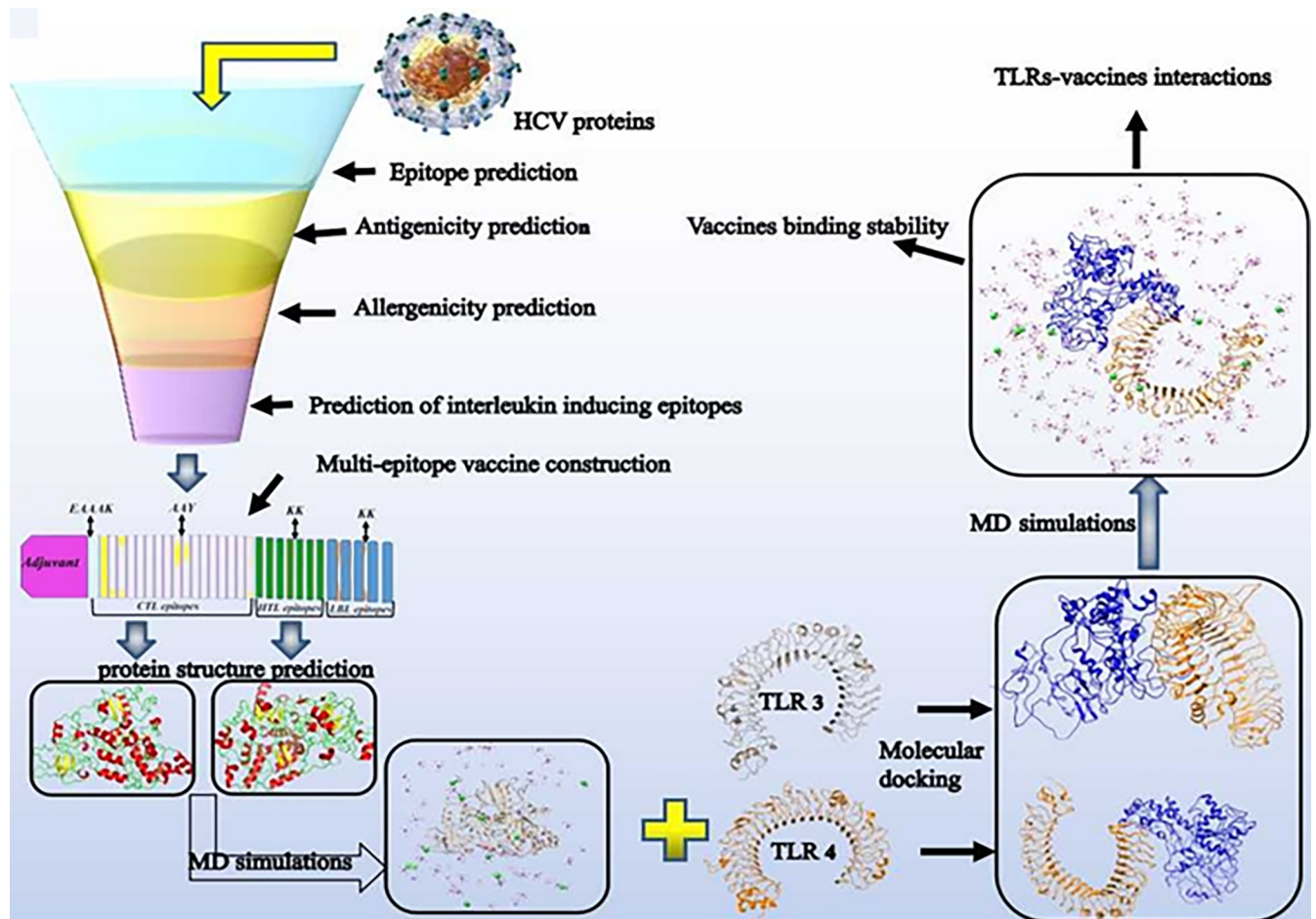


Fig 1. Systemic flowchart of the multi-epitope subunit vaccines build against HCV.

<https://doi.org/10.1371/journal.pone.0272582.g001>

2.1. Viral protein sequences

For designing multi-epitope vaccine constructs against HCV, both structural and non-structural protein sequences were obtained from protein databases. The occurrence of high mutation rate in the HCV genome in infected populations facilitates immune escape and adaptation of the virus. Therefore, to obtain a vaccine active against wide range of viral strains, alignment of the viral protein sequences from various strains is needed to gain conserved sequences in order to select efficient candidate epitopes. To this aim, clustalW2 was used to perform multiple sequence alignment [27].

2.2. Prediction of MHC-I binding (Cytotoxic T Lymphocyte (CTL)) epitopes

Predicting peptides that are capable of inducing T-cell responses is a crucial step in the design of epitope-based peptide vaccine. The NetCTL v1.2 server (www.cbs.dtu.dk/services/NetCTL) was applied to predict the CD8+ T-cell epitopes. In the IEDB MHC class I binding tool (www.iedb.org), the Artificial Neural Network and human were selected as prediction method and MHC source species, respectively. The IC50 value was selected 50 nM. In the NetCTL v1.2 server, the threshold value was selected as 0.5.

2.3. Prediction of MHC-II binding (Helper T Lymphocyte (HTL)) epitopes

The IEDB tool was used to predict HTL epitopes in structural and non-structural proteins of the HCV. Then, HTL epitopes with IC50 value of less than 50 nM were selected for further use.

2.4. Prediction of linear B-cell epitopes

As we know, one of the important factors in the process of immunization of the human body against pathogens is the secretion of antibodies by B lymphocytes, participating in the humoral immunity. In this study, BCPred server (<http://ailab.ist.psu.edu/bcpred>) was utilized to predict 20-mer B-cell epitopes, using a support vector machine (SVM) algorithm and a kernel technique.

2.5. Estimation of antigenicity, allergenicity, and toxicity of CTL, HTL and B cells epitopes

The antigenic potential of CTL, HTL and B cells epitopes was predicted using the VaxiJen v2.0, and epitopes with antigenic values of more than 0.4 were selected for further screening [28]. The toxicity and allergenicity of these selected epitopes were checked by the ToxinPred and the AllerTOP servers, respectively [29, 30]. Subsequently, the ability to induce the secretion of various interleukins (interferon-gamma (IFN- γ), interleukin-4 (IL-4) and interleukin-10 (IL-10) secreted by B and HTL (CD4⁺) cells epitopes was checked through the IFNepitope, IL4pred and IL10pred server tools [31–33]. Among the predicted epitopes, those with high antigenic potential, non-allergenicity and non-toxicity and high solubility at high expression levels were selected to develop a multi-epitope vaccine.

2.6. Designing of multi-epitope vaccine construct

The multi-epitope vaccine was designed via fusion of CTL, HTL and B cells epitopes with appropriate linkers (AAY and KK) according to recent studies [15–19]. Two separate adjuvants were also added to the N termini to increase the immunogenicity of the multi-epitope vaccines [15–19]. To this aim, a 124- and a 45-amino acid sequences from 50S ribosomal protein L7/L12 (TLR4 agonist) and human β -defensin 2 (TLR3 agonist) were respectively obtained and added separately to the N terminus of the vaccine sequence using the appropriate linker (EAAAK) [15]. The vaccines designed in this route contained 686 and 607 residues, respectively.

2.7. Estimation of immunogenic, allergenic and physicochemical properties of multi-epitope vaccines

The VaxiJen v2.0 and SolPro (<http://scratch.proteomics.ics.uci.edu/>) web tools were used to predict the antigenic potential and solubility of the multi-epitope vaccines, respectively [28]. The allergenicity of the vaccines was checked using AllerTOP server [29]. In addition, the physicochemical properties of the vaccines, such as amino acid composition, theoretical isoelectric point (pI), grand average of hydropathicity (GRAVY), molecular weight, aliphatic and instability index, and *in vitro* and *in vivo* half-life were evaluated using ProtParam server [34].

2.8. Modeling the three-dimensional structure of the multi-epitope vaccines

The secondary structural properties of the multi-epitope vaccine were analyzed using the SOPMA secondary structure prediction method [35]. Modeling and refinement of the three-dimensional (3D) structure of the multi-epitope vaccines was performed using the Galaxy server (<http://galaxy.seoklab.org/>). The Galaxy server relaxes the model structure using repacking and molecular dynamics simulation. The 3D structure of the multi-epitope vaccines was then validated using a variety of tools, such as SWISS-MODEL server [36], ProSA-web [37] and ERRAT (<https://servicesn.mbi.ucla.edu/>).

2.9. Molecular dynamics simulation of multi-epitope vaccines

High-performance MD simulation is an important method to validate the stability of the modeled structures. The multi-epitope vaccines and vaccine-TLRs complexes were simulated for 100 ns using Gromacs 2020 package [38], implementing similar protocols as in our previous studies [39]. The simulation trajectories were saved for the multi-epitope vaccines and complexes every 10 ps and root mean square deviations (RMSDs), root mean square fluctuations (RMSFs) and radius of gyration (Rg) analyses were carried out by Gromacs tools box. The final structures of multi-epitope vaccines were used as a ligand for docking to TLR3 and TLR4.

2.10. Molecular docking of toll-like receptors and multi-epitope vaccines

The molecular docking of the final vaccines after 100 ns simulations with TLR3 (PDB ID: 2A0Z) and TLR4 (PDB ID: 4G8A, www.rcsb.org) was performed using the ClusPro 2.0 web server [40] to analyze the binding pattern of vaccines with TLR3 and TLR4. Based on the lowest global energy, the final vaccine-TLRs complexes models were selected and visualized using PyMOL package and LIGPLOT software [41, 42].

3. Results

3.1. Sequence alignment

The alignment of various HCV protein sequences was performed using ClustalW2 (<https://embnet.vital-it.ch/software/ClustalW.html>). The results of this step has been shown in supplementary data.

3.2. Prediction and evaluation of HTL, CTL and B cell epitopes

The IEDB MHC-II prediction tool, the NetCTL 1.2 and the BCPred servers were used to predict HTL (15-mer), CTL and B-cell linear epitopes of the HCV proteins, respectively (S1–S9 Tables). The potentially antigenic and non-allergenic epitopes (using VaxiJen v2.0 and AllerTOP v.2.0, respectively) were adopted and next, those induced various cytokines such as IFN- γ , IL-4, and IL-10 (via prediction of B and HTL epitopes) were obtained (Table 1).

3.3. Combining selected epitopes to make the final multi-epitope vaccine

Selected potential epitopes including 18 CTL, 7 HTL and 5 LBL epitopes were fused together using AAY and KK linkers, respectively (Fig 2A). The 50S ribosomal protein L7/L12 (TLR4 agonist) and human β -defensin 2 (TLR3 agonist) adjuvants were separately added to the N-terminal part sequence of the final multi-epitope vaccine using an EAAAK linker to increase immunogenicity (Fig 2A) giving final multi-epitope vaccines sequences with 686 and 607 residues (S1 Fig).

Table 1. Final selected CTL, HTL and LBL epitopes for multi-epitope vaccines construction.

Protein	CD8+-T cell epitope	CD4+-T cell epitope	B-cell epitope
P7	⁴² YAIYGTWPL	³⁶ LVPGMTYAIYGTWPLLL	³² IKGRLVPGMTYAIYGTWPLL
	⁵⁴ LLALPQRAY		
NS3	⁴³² VTQTVDFSLDPTFTI	⁵⁰⁰ AWYELTPAETTVRLR	⁵⁸⁷ RLKPTLRGPTPLLY
	¹²⁶ LLSPRPVSY		
	²⁰⁴ APTGS GKST		
	³⁶² GRHLIFCHSKKK		
	¹²³ RGSLSPRPVSYLK		
	¹⁰⁷ VTRHADVIPV		
	³⁸³ GLGINAVAY		
	²⁶² GAPITYSTY		
NS5B	²³⁰ PSVAATLGFAYMSKAH	⁵⁶⁰ IYHSLRARPRWFMW	¹⁴¹ KSEVFCVQPEKGGR
	⁴⁵⁴ IEPLDLPQI		
	⁴⁸⁹ LRKLGVPPLR		
	¹³² TPIDTTIMAKSEVFCVQPEK		
	⁵⁶⁰ IYHSLRARPRWFMWCLLLSVGVGIYL		
	⁵⁰⁰ WRHRARSVRARLLSQGGAATCGKYLFNWAVRTKCLKLTP		
	¹⁹⁹ QRVEFLVNAWKS KSPMGFSYDTRCFDSTVTESDIRV		
²⁹ SLLRHHNMVYATTRSASLRQKKVTF	³⁵ NMVYATTSRASLRQ		

<https://doi.org/10.1371/journal.pone.0272582.t001>

3.4. Evaluation of antigenicity, allergenicity, physicochemical properties and secondary structure of the vaccine constructs

The designed vaccines were sufficiently antigenic and non-allergenic. Their molecular weight included 76.27 kDa and 67.87 kDa, and their theoretical pI included 9.98 and 10.16 (Table 2). The instability and the aliphatic indices of the final vaccines have been represented in the Table 2. The final vaccines have a grand average of hydrophobicity (GRAVY) values of -0.152 and -0.169 (Table 2 and S1 Fig).

3.5. Modeling, refinement, and validation of vaccine constructs

The three-dimensional structures of the final vaccines were modeled and refined (Fig 2). In the optimal structural model of construct 1, 91.08% of the residues were in the favored area, 7.17% in the allowed area and 1.75% in the disallowed area of Ramachandran plot (Fig 2B). In addition, the quality factor obtained from the ERRAT analysis was 76.41% and the Z-score was -3.28 (Fig 2C). Regarding the construct 2, 91.07% of the residues were in the favored area, 7.28% in the allowed area and 1.65% in the disallowed area of Ramachandran plot (Fig 2D). In addition, the quality of 72.64% and the Z-score of -3.88 was obtained (Fig 2E). The ERRAT score included 76.41% and 72.64% for the vaccine candidates (Fig 3F and 3G).

3.6. Prediction of B-cell epitopes in the final vaccines

In general, four discontinuous B-cell epitopes with score of 0.83 to 0.87, and 12 linear B-cell epitopes with score of 0.83 to 0.93 were selected as the final epitopes in 50S ribosomal protein L7/L12-multi-epitope vaccine (S2 Fig, Tables 3 and 4). In addition, six discontinuous B-cell epitopes with score range of 0.82 to 0.88, and 14 linear B-cell epitopes with score range of 0.83 to 0.91 were selected as the final epitopes in human β -defensin 2-multi-epitope vaccine (S2 Fig, Tables 3 and 4). For both multi-epitope vaccines, the PI values of 0.87 and 0.88

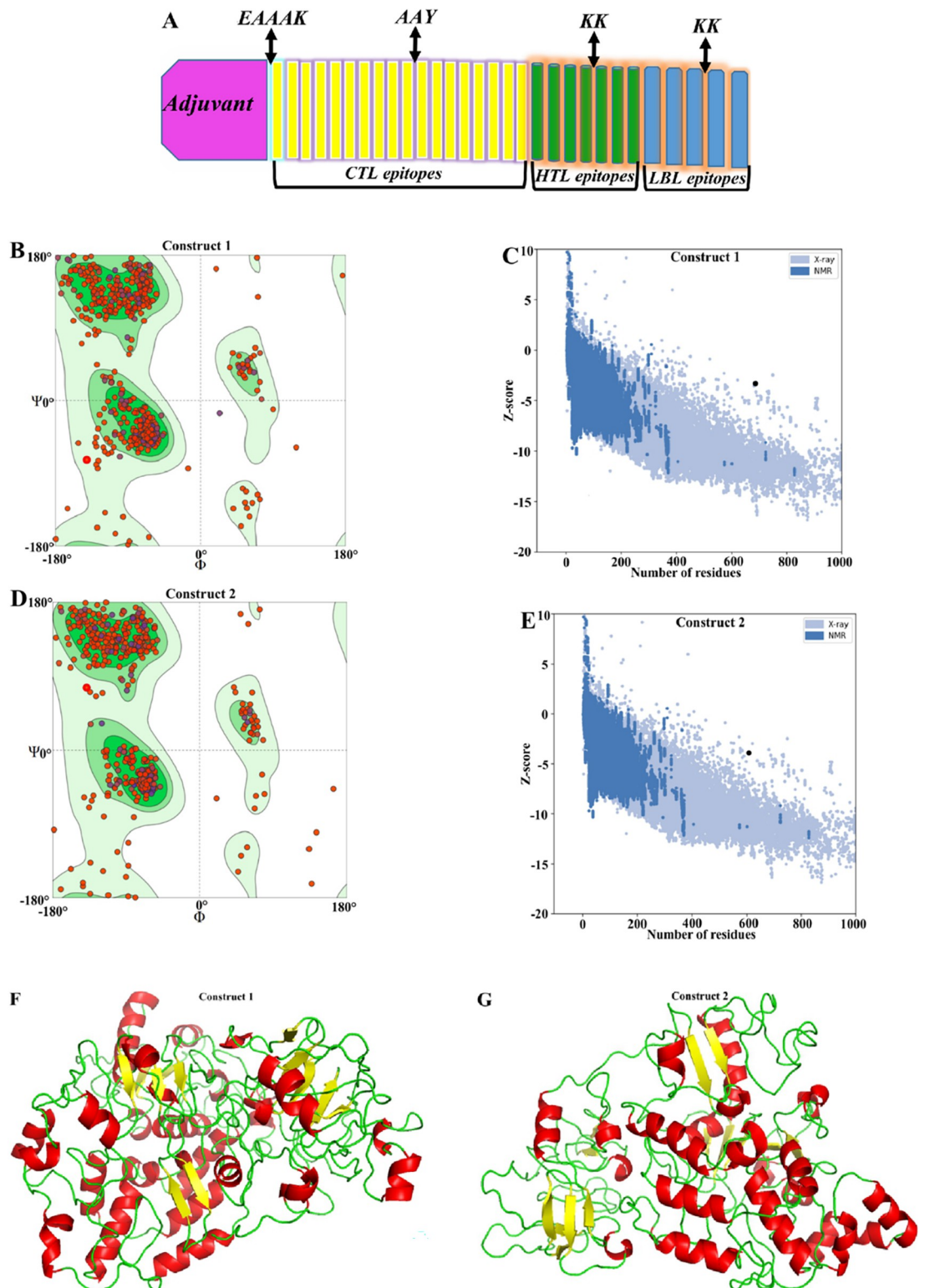


Fig 2. Prediction and assessment of the 3D structure of the multi-epitope vaccines. (A) Schematic image of the final vaccine. (B) Ramachandran plot analysis of refined construct 1, showing 91.08%, 7.17% and 1.75% residues in favored, allowed and disallowed region, respectively, (C) ProSA validation of 3D construct 1, showing Z-score -3.28, (D) Ramachandran plot analysis of refined construct 2, showing 91.07%, 7.28% and 1.65% residues in favored, allowed and disallowed region, respectively, (E) ProSA validation of 3D construct 2, showing Z-score -3.88, (F and G) 3D structure of vaccines models showing α -helix (red cartoon), β -strand (yellow cartoon) and loop (green cartoon).

<https://doi.org/10.1371/journal.pone.0272582.g002>

Table 2. Various features of multi-epitope vaccines.

Features	Assessment	
	Construct 1	Construct 2
Adjuvant	50S ribosomal protein L7/L12 (TLR4)	Human β -defensin 2 (TLR3)
Number of amino acids	686	607
Molecular weight	76270.36 Dalton	67872.61 Dalton
Chemical formula	C3496H5551N933O938S19	C3104H4887N851O811S24
Theoretical pI	9.98	10.16
Total number of negatively charged residues (Asp + Glu):	43	24
Total number of positively charged residues (Arg + Lys)	107	97
Total number of atoms	10937	9677
Extinction coefficient (at 280 nm in H ₂ O)	126060 M ⁻¹ cm ⁻¹	127550 M ⁻¹ cm ⁻¹
Instability index	35.01	38.13
Aliphatic index	89.55	81.76
Grand average of hydropathicity (GRAVY)	-0.152	-0.169
Antigenicity	0.53 (AntigenPro), 0.75 (Vaxijen v.2.0)	0.80 (AntigenPro), 0.78(Vaxijen v.2.0)
Allergenicity	Probable non-allergen (AllergenFP v.1.0)	Probable non-allergen (AllergenFP v.1.0)
	Probable non-allergen (AllerTOP v.2.0)	Probable non-allergen (AllerTOP v.2.0)

<https://doi.org/10.1371/journal.pone.0272582.t002>

demonstrated that 87% and 88% of residues located in the predicted ellipsoid area of the epitopes and these epitopes had the highest solvent accessibility.

3.7. Molecular dynamic simulation of multi-epitope vaccines

The RMSD of the constructs C α atoms raise up over time which highlighted a continues increasing trend up to 25 ns and next reached a plateau indicating a stable structural conformations, while the RMSD value converged within ~1 nm (Fig 3A) Likewise, the C α -RMSF graph of the constructs during 100 ns of MD simulation was identified as stable dynamics behavior (Fig 3B). However, higher fluctuation rates were observed in the loop regions. The similar patterns of the RMSD and RMSF and low changes at various time intervals, revealed good structural stability of the vaccine constructs.

3.8. Molecular docking of the immune receptors (TLRs) with adjuvant and vaccines

A diverse hydrophobic and hydrophilic interactions participated in the adjuvants-TLRs binding (S3 Fig). Moreover, the molecular docking of the final vaccines after 100 ns simulations with TLR3 (PDB ID: 2A0Z) and TLR4 (PDB ID: 4G8A) was performed (S4 Fig). Next, the complex with best ClusPro score was selected and further applied for running MD simulation investigations.

3.9. Molecular dynamic simulation of multi-epitope vaccines-TLRs complexes

The molecular dynamics simulations of the docked complexes were performed for 100 ns. These simulations studies are capable to address several important queries about the structural stability of the final complexes. To address these queries, it is warranted to assess several main statistical factors based on MD simulation outputs (Fig 3C–3G).

The conformational stability of the vaccines and TLRs in the complexes states was investigated based on the calculation of the overall fluctuations of the final vaccines. The RMSD values were calculated as a time-dependent parameter for decoding the displacement of C α

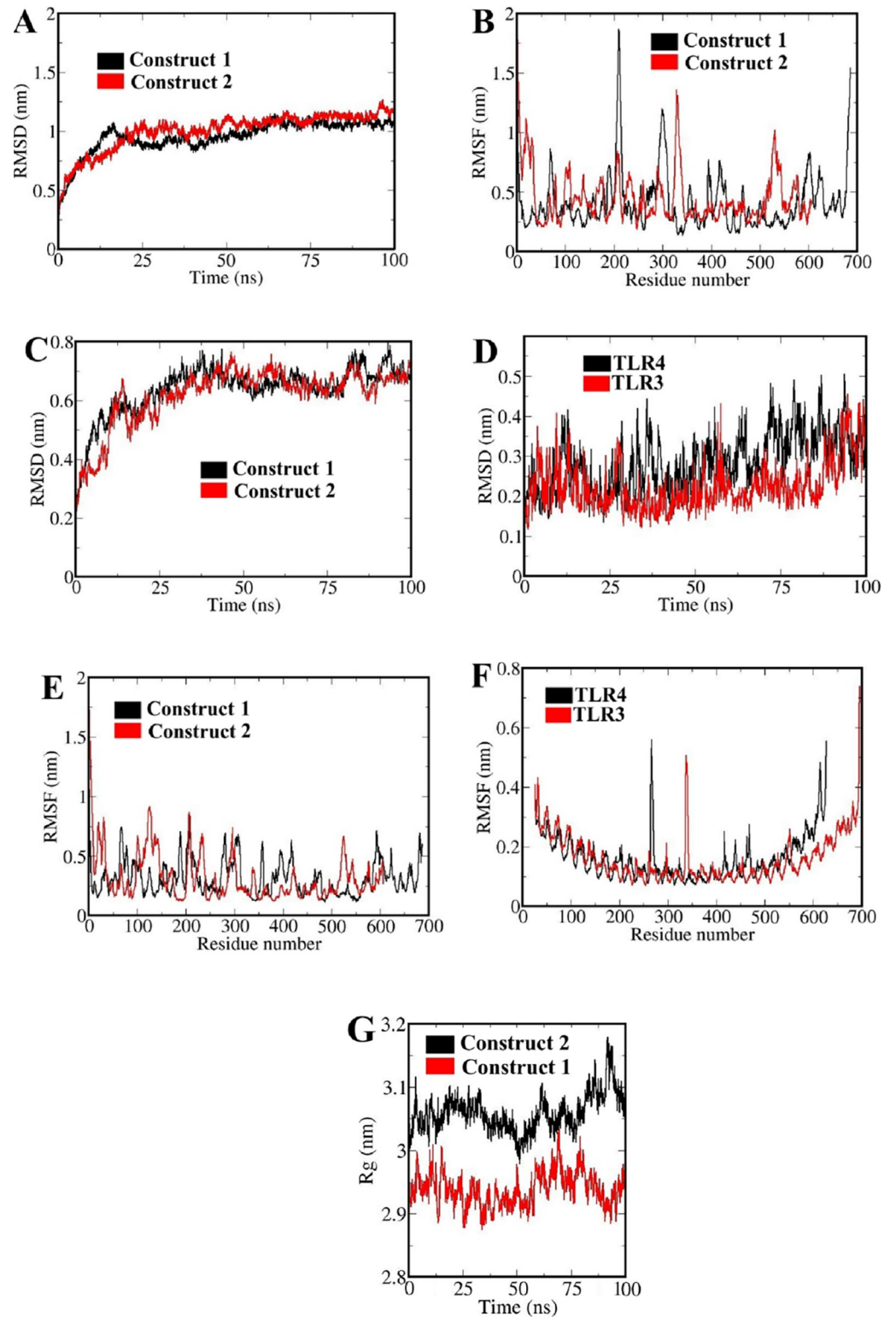


Fig 3. MD simulations outputs of free vaccines and vaccines-TLRs complexes; A and B: The RMSD and RMSF values of C α atoms for free vaccines, respectively; C and D: The RMSD values of C α atoms for vaccines and TLRs in the complex states, respectively; E and F: The RMSF values of C α atoms for vaccines and TLRs in the complex states, respectively; G: The Rg values of vaccines structures in the complex states.

<https://doi.org/10.1371/journal.pone.0272582.g003>

Table 3. Linear B-cell epitopes of the final vaccines.

	Linear B cell epitopes	Score
Construct 1	²⁵⁰ AAYGAPITYS ²⁵⁹	0.93
Construct 1	³⁰⁶ RAAYTPID ³¹³	0.91
Construct 1	⁶² LKGAGS ⁶⁷	0.91
Construct 1	⁷⁰ LTVVKRIKDLIGL ⁸²	0.90
Construct 1	²⁷⁸ SKAHAAYIEPLDL ²⁹⁰	0.90
Construct 1	⁶¹⁴ AIYGTWPLLKRLKPTLRGPT ⁶³⁴	0.89
Construct 1	⁶⁴⁵ TDNSTPP ⁶⁵¹	0.88
Construct 1	⁵⁶² ARAQAPK ⁵⁶⁸	0.88
Construct 1	⁴⁵ KAEILDKS ⁵²	0.87
Construct 1	⁵⁸⁹ VYATTS ⁵⁹⁴	0.85
Construct 1	³⁵⁶ VGIYLAAYW ³⁶⁴	0.85
Construct 1	⁶⁰⁶ RLVPGM ⁶¹¹	0.83
Construct 2	¹ GIINTLQKYYCRVRGGRC ¹⁸	0.91
Construct 2	⁵²¹ RQKKKGRLVPGMTYAIYGTW ⁵⁴⁰	0.89
Construct 2	¹⁹⁹ SKAHAAYIEPLDLPQIA ²¹⁵	0.88
Construct 2	²²⁵ PLRAAYTPI ²³³	0.86
Construct 2	²³⁷ IMAKSE ²⁴²	0.86
Construct 2	⁹⁴ PVSYAAYAPTGSKGKSTA ¹¹⁴	0.85
Construct 2	⁵⁷² PAVPKKPA ⁵⁷⁹	0.85
Construct 2	⁵⁴⁹ PTLRG ⁵⁵³	0.84
Construct 2	³³⁹ SKKS ³⁴²	0.82
Construct 2	⁵¹¹ YATTS ⁵¹⁵	0.82
Construct 2	⁶⁶ LPQRA ⁷⁰	0.81
Construct 2	¹⁷⁶ PITYS ¹⁸⁰	0.81
Construct 2	²⁵⁹ SRARPRW ²⁶⁵	0.81
Construct 2	²² SCLPKEEQ ²⁹	0.80

<https://doi.org/10.1371/journal.pone.0272582.t003>

atoms in the final vaccine constructs and TLRs during simulation times (Fig 3C and 3D). Fluctuations in the vaccine's RMSD graph could be due to the movement of the residues to achieve a suitable and stable conformation of the vaccines in the complexes states. The RMSD fluctuations of the vaccines structures in the complexes states were lower than free states vaccines, which indicated the stability of the vaccines structures during complexes simulations (Fig 3). In addition, the RMSD graph of the TLRs structures in the complexes states were low and smooth, which indicated their structural stability in the complexes states (Fig 3).

Local structural fluctuations were estimated utilizing the RMSF factor for the vaccines and TLRs structures during the complexes simulations (Fig 3E and 3F). Loop areas exhibited highest fluctuations in the complexes states. The RMSF graph of the TLRs showed low flexibility, which clarified that TLRs had good structural stability in the complexes states (Fig 3F).

The high value of Rg (Fig 3G) indicates a decrease in protein compactness. Fluctuations in the Rg diagram indicate the movements of the vaccines domains which induce conformational changes and thereby select a suitable conformation in the complexes states. Hence, the studied complexes had a proper structural stability.

3.10. Estimation of binding free energy of immune receptor-vaccine complex

Both hydrophilic (ΔE_{polar}) and hydrophobic energy terms ($\Delta E_{\text{nonpolar}}$) were participated in the binding of vaccines to the TLRs (Table 5). However, hydrophilic energy was as main driving

Table 4. Discontinuous B-cell epitopes of the final vaccines.

Discontinuous B cell epitopes	Number of residues	Score	
A:A250, A:A251, A:Y252, A:G253, A:A254, A:P255, A:I256, A:T257, A:Y258, A:S259, A:A275, A:S278, A:K279, A:A282, A:A283, A:Y284, A:I285, A:E286, A:P287, A:L288, A:D289, A:L290, A:P291, A:Q292, A:R306, A:A307, A:A308, A:Y309, A:T310, A:P311, A:I312, A:D313, A:V356, A:G357, A:I358, A:Y359, A:L360, A:A361, A:A362, A:Y363, A:W364, A:H366, A:R367, A:A368, A:R369	45	0.87	Construct 1
A:A562, A:R563, A:A564, A:Q565, A:A566, A:P567, A:K568, A:Y571, A:K586, A:P620, A:L621, A:L622, A:K623, A:K624, A:R625, A:L626, A:K627, A:P628, A:T629, A:L630, A:R631, A:G632, A:P633, A:T634, A:P635, A:L636, A:T645, A:D646, A:N647, A:S648, A:T649, A:P650, A:P651	33	0.87	Construct 1
A:K45, A:A46, A:E47, A:I48, A:L49, A:D50, A:K51, A:S52, A:D59, A:I61, A:L62, A:K63, A:G64, A:A65, A:G66, A:S67, A:L70, A:T71, A:V72, A:V73, A:K74, A:I76, A:K77, A:D78, A:L79, A:I80, A:G81, A:L82, A:G83, A:L84, A:K85, A:E86, A:S87, A:K88, A:D89, A:V91, A:D92, A:K96, A:K100, A:G101, A:L102, A:S103, A:K104, A:E105, A:E106, A:A107, A:E108, A:S109, A:L145, A:P146, A:Q147, A:R148, A:P177, A:V178, A:S179, A:Y180	56	0.84	Construct 1
A:R580, A:V589, A:Y590, A:A591, A:T592, A:T593, A:S594, A:A597, A:Q601, A:K602, A:A614, A:I615, A:Y616, A:G617, A:T618, A:W619	16	0.83	Construct 1
A:V510, A:Y511, A:A512, A:T513, A:T514, A:S515, A:A518, A:R521, A:K523, A:K524, A:G526, A:R527, A:L528, A:V529, A:P530, A:G531, A:M532, A:T533, A:Y534, A:A535, A:I536, A:G538, A:T539, A:W540, A:R546	25	0.88	Construct 2
A:V13, A:G15, A:G16, A:R17, A:C18	5	0.87	Construct 2
A:S180, A:S199, A:K200, A:A203, A:A204, A:Y205, A:I206, A:E207, A:P208, A:L209, A:D210, A:L211, A:P212, A:Q213, A:I214, A:A215, A:A216, A:V223, A:P224, A:P225, A:L226, A:A228, A:A229, A:Y230, A:T231, A:P232, A:I233, A:D234, A:T236, A:I237, A:M238, A:A239, A:K240, A:S241, A:E242	35	0.84	Construct 2
A:G1, A:I2, A:I3, A:N4, A:T5, A:L6, A:Q7, A:K8, A:Y10, A:C11, A:R12, A:R14, A:S22, A:C23, A:L24, A:P25, A:K26, A:E27, A:E28, A:Q29, A:C41, A:K44, A:K45, A:A65, A:R97, A:P98, A:V99, A:S100, A:Y101, A:A102, A:A103, A:L120	32	0.84	Construct 2
A:A485, A:Q486, A:A487, A:P549, A:T550, A:L551, A:R552, A:P572, A:A573, A:V574, A:P575, A:K576, A:K577, A:P578, A:A579, A:Q581	16	0.83	Construct 2
A:R42, A:Y104, A:A105, A:P106, A:T107, A:G108, A:S109, A:G110, A:K111, A:S112, A:T113, A:A114, A:H124, A:K126, A:K128, A:A129, A:L136, A:S137, A:P138, A:R139	20	0.82	Construct 2

<https://doi.org/10.1371/journal.pone.0272582.t004>

force in the interactions between the immune receptors and the vaccines, compared to hydrophobic energy. Paramount residues which were participated at the interface regions have been identified (Fig 4). Accordingly, both polar and non-polar residues played key roles at the binding process, of the vaccines-TLRs complexes (Fig 4).

Table 5. The contribution of various energy components in the ΔG_{bind} (kJ/mol).

	Construct 1-TLR 4	Construct 2-TLR 3
ΔE_{ele}^a	-15786.76 ± 490.57	-11730.95 ± 240.61
ΔE_{vdw}^b	-460.52 ± 87.34	-247.89 ± 68.97
ΔG_{PB}^c	1476.22 ± 249.39	2323.25 ± 429.45
ΔG_{SA}^d	-64.67 ± 8.02	-45.45 ± 8.03
$\Delta E_{non-polar}^e$	-525.19 ± 47.68	-9407.7 ± 335.03
ΔE_{polar}^f	-14310.54 ± 369.95	-293.34 ± 38.5
ΔG_{bind}	-14835.73 ± 208.82	-9701.04 ± 186.76

^aElectrostatic connection

^bvan der Waals connection

^cPolar contribution of the solvation effect

^dNon-polar contribution of solvation effect

^e $\Delta E_{non-polar} = \Delta E_{vdw} + \Delta G_{SA}$

^f $\Delta E_{polar} = \Delta E_{ele} + \Delta G_{PB}$

<https://doi.org/10.1371/journal.pone.0272582.t005>

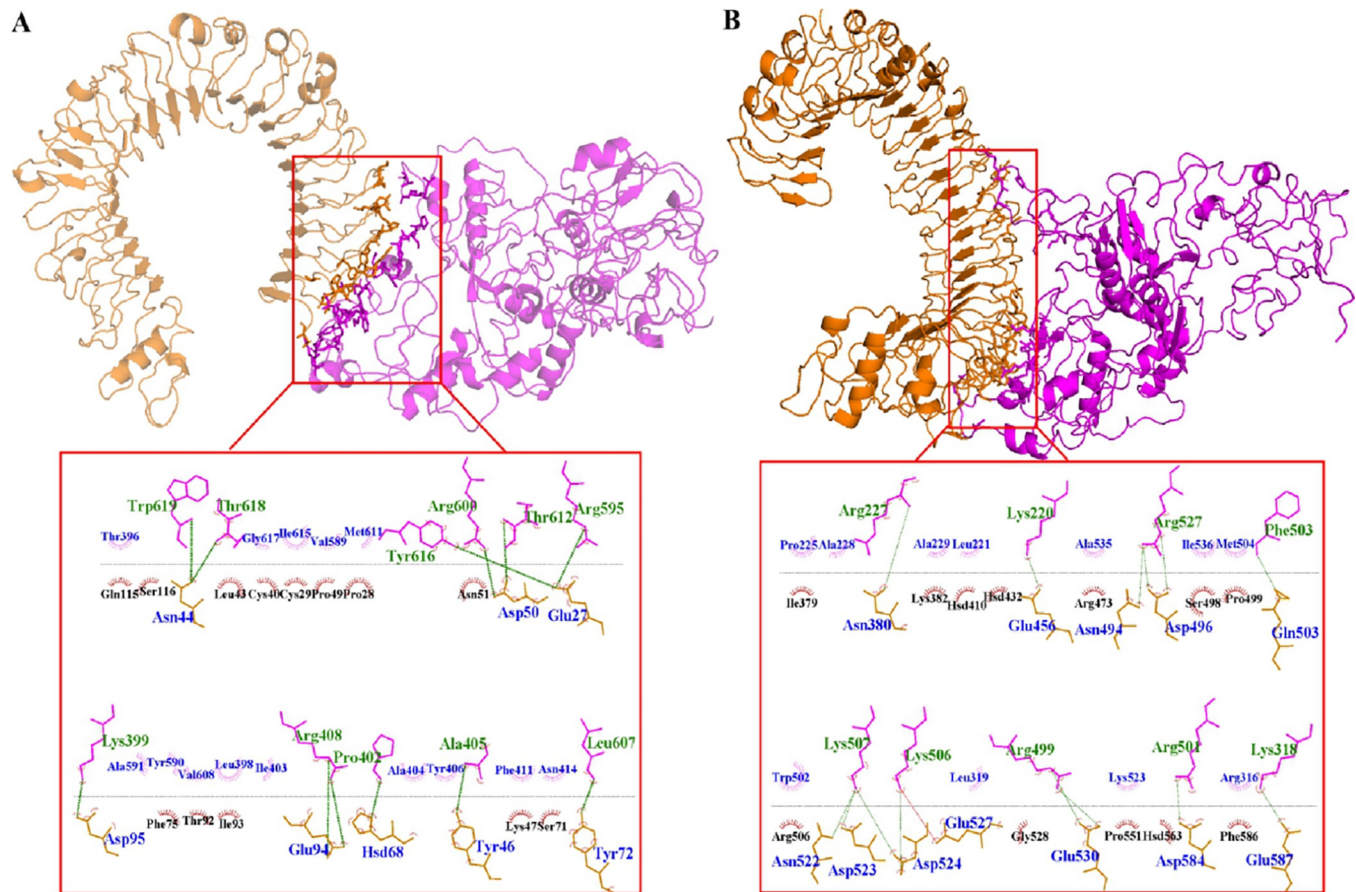


Fig 4. The 3D view of the final system conformations. The interface residues between two proteins TLRs (orange cartoon) and vaccines (magenta cartoon) residues (orange and magenta sticks) are labeled. Hydrogen bonds and hydrophobic contacts are presented as green dashed line and arc with spokes radiating, respectively. A and B indicate TLR4-construct 1 and TLR3-construct 2 complexes, respectively.

<https://doi.org/10.1371/journal.pone.0272582.g004>

4. Discussion

Following the HCV protein sequences alignment, we used the IEDB MHC-II prediction tool, the NetCTL 1.2 and the BCPred servers to predict HTL (15-mer), CTL and B-cell linear epitopes, respectively (S1–S9 Tables). Those antigenic and non-allergenic epitopes were adopted and next those antigenic B and HTL epitopes were used for the construction of our multi-epitope vaccines (Table 1).

Selected epitopes containing 18 CTL, 7 HTL and 5 LBL epitopes were fused together using AAY and KK linkers, respectively (Fig 2A). Two adjuvants including 50S ribosomal protein L7/L12 (TLR4 agonist) and human β -defensin 2 (TLR3 agonist) were added separately to the N terminal domain of the final multi-epitope vaccine using an EAAAK linker to increase immunogenicity (Fig 2A), synthesizing constructs with 686 and 607 residues (S1 Fig). These designed vaccines were also potentially antigenic and non-allergenic. Their molecular weight included 76.27 kDa and 67.87 kDa, and their theoretical pI were 9.98 and 10.16 (Table 2), which indicates the basic nature of the vaccines. The instability and the aliphatic indices of the final vaccines have been represented in the Table 2, which indicates their appropriate structure and high thermo-stability. The final vaccines also deciphered a grand average of hydrophobicity (GRAVY) values of -0.152 and -0.169, confirming their hydrophilic characters (Table 2).

Therefore, they can interact with other proteins and are soluble in water. The predicted secondary structure of the final vaccine has been exhibited in the [S1 Fig](#).

Galaxy server, SWISS-MODEL, ProSA-web and ERRAT servers ([Fig 2](#)) demonstrated that in the best three-dimensional structural model of the construct 1, 91.08% of the residues placed in the favored area, 7.17% in the allowed area and 1.75% in the disallowed area of Ramachandran plot ([Fig 2B](#)). In addition, the quality factor obtained from the ERRAT analysis was 76.41% and its Z-score was -3.28 ([Fig 2C](#)). Regarding the construct 2, 91.07% of the residues were in the favored area, 7.28% in the allowed area and 1.65% in the disallowed area of Ramachandran plot ([Fig 2D](#)). In addition, the quality factor and Z-score included 72.64% and -3.88 , respectively ([Fig 2E](#)). A $\geq 90\%$ reliability cut-off is mandatory for residues placing in the favoured region [43] which was confirmed in our study. The ERRAT score of 76.41% and 72.64% for the vaccine constructs clarified the adequate quality and validity percentage. An ERRAT score >50 indicates a suitable quality model [44]. All of these indicators confirm the good quality of the 3D structures of the final vaccines ([Fig 3F and 3G](#)).

We observed four discontinuous B-cell epitopes with a score of 0.83 to 0.87, and 12 linear B-cell epitopes with a score of 0.83 to 0.93, selected as the final epitopes in 50S ribosomal protein L7/L12-multi-epitope vaccine ([S2 Fig](#), [Tables 3 and 4](#)). In addition, six discontinuous B-cell epitopes with score of 0.82 to 0.88, and 14 linear B-cell epitopes with score of 0.83 to 0.91 were selected as the final epitopes in human β -defensin 2-multi-epitope vaccine ([S2 Fig](#), [Tables 3 and 4](#)). For both multi-epitope vaccines, the PI values of 0.87 and 0.88 demonstrated that 87% and 88% of residues located in the predicted ellipsoid area of the epitopes, having the highest solvent accessibility. Following the MD simulations for 100 ns, in the RMSD of the constructs, $C\alpha$ atoms raise up over time which highlighted a continues increasing trend up to 25 ns and then reaching a plateau which indicated a stable structural conformations, while the RMSD value converged within ~ 1 nm ([Fig 3A](#)). Likewise, the $C\alpha$ -RMSF graph of the constructs deciphered stable dynamics behavior ([Fig 3B](#)). However, higher fluctuation rates were observed in the loop regions. Similar patterns of the RMSD and RMSF and low changes at various time intervals, revealed good structural stability of the vaccine constructs. These final constructs were used as the ligands for docking to the TLRs. The molecular docking demonstrated the interaction of the TLRs with the adjuvants. Accordingly, a diverse hydrophobic and hydrophilic interactions participated in the adjuvants-TLRs binding ([S3 Fig](#)).

Moreover, the molecular docking of the final vaccines after 100 ns simulations with TLR3 (PDB ID: 2A0Z) and TLR4 (PDB ID: 4G8A) was performed ([S4 Fig](#)). The simulations studies were capable of addressing main queries regarding the structural stability of the final complexes depicted as outputs ([Fig 3C–3G](#)).

The conformational stability of the vaccines and TLRs in the complexes states was investigated based on the calculation of the overall fluctuations of the final vaccines. The RMSD values were calculated as a time-dependent parameter for decoding the displacement of $C\alpha$ atoms in the final vaccine constructs and TLRs during simulation times ([Fig 3C and 3D](#)). Fluctuations in the vaccine's RMSD graph could be due to the movement of the residues to form a suitable and stable conformation of the vaccines in the complexes states, being lower than free states vaccines, which indicated the stability of the vaccines structures during complexes simulations ([Fig 3](#)). In addition, the RMSD graph of the TLRs structures in the complexes states were low and smooth, which indicated their structural stability in the complexes states ([Fig 3](#)).

Local structural fluctuations estimation utilizing the RMSF factor ([Fig 3E and 3F](#)) revealed highest fluctuations of loop areas in the complexes states. These localized fluctuations in vaccines residues can facilitate vaccine epitopes' exposure to TLRs and make sufficient space for side chains to adopt suitable conformation for binding to TLRs. The RMSF graph of the TLRs

showed low flexibility, clarifying their sufficient structural stability in the complexes states (Fig 3F).

The high value of Rg indicates a decrease in protein compactness. Fluctuations in the Rg diagram indicate the movements of the vaccines domains which induce conformational changes and thereby select a suitable conformation in the complexes states. According to the pattern of changes in these factors, our vaccines structures system displayed high stability during complexes simulations (Fig 3G). Accordingly, the multi-epitope vaccines-TLRs constructs achieved a suitable and stable conformational complexes during the simulations times, highlighting their proper structural stability.

The binding free energy profile of our vaccine candidates (Table 5) [45] revealed that both hydrophilic (ΔE_{polar}) and hydrophobic energy terms ($\Delta E_{\text{nonpolar}}$) participated in the binding of vaccines to the TLRs. However, hydrophilic energy was the main driving force in the interactions, compared to hydrophobic energy (Fig 4). Accordingly, both polar and non-polar residues played key roles in the binding process, of the vaccines-TLRs complexes (Fig 4).

Noticeably, the output of the TLRs-vaccines complexes outlined the high structural stability of molecular species docked together during the simulation. Hydrophilic residues play a vital role in the interactions between the vaccines and the TLRs, which in turn determine high stability of the complex structure. Indeed, these binary interactions cause the efficient adhesion of molecular species together. Accordingly, the vaccine candidate constructs had the ability to stimulate the immune system's responses efficiently though further studies are warranted to verify these findings in vitro and in vivo. In previous studies multi-epitope vaccine constructs have been used against *Leishmania donovani* stimulating CD8+ T cells and INF γ (19 antigenic proteins, 49 epitopes binding to 40 different MHC class I supertypes) [46], provoking CD8+ T cells (LeIF and TSA) [47] and induction of CD4+, CD8+, IFN- γ and IL-10 [48]. Major limitations of our survey included lack of experimental assessment of the multi-epitope vaccine in vitro, in vivo or in clinical trial. A study using multi-epitope DNA- and peptide-based vaccines provoked CD4+ and CD8+ responses against the HCV and were evaluated in BALB/c mice model [49].

5. Conclusion

The efficient anti-HCV treatment approaches are limited due to various side effects, recurrency and antiviral resistance development. Thereby, it is essential to seek other strategies like vaccine design. Currently, it is possible to design recombinant and multi-epitope vaccines more rapid and cost effective using a variety of computational methods. Accordingly, we attempted to design multi-epitope vaccine candidates based on the conserved areas of the HCV structural and non-structural protein sequences using the immunoinformatics tools. According to our findings, the vaccines constructs (including CTL, HTL and B cell epitopes plus two adjuvants or TLR3 and TLR4 agonists) were efficient in terms of antigenicity, non-toxicity, solubility, immunogenicity, non-allergenicity and stability. The 3D structures of the multi-epitope vaccine candidates' models were highly stable and soluble. Additionally, their interactions with the TLR3 and TLR4 resulted in efficient vaccine candidates with acceptable traits in silico. Our computational findings were promising considering the candidate multi-epitope vaccines potential in controlling the HCV infection.

Supporting information

S1 Table. Linear B cell (LBL) epitopes of the P7 protein.
(DOCX)

S2 Table. Linear B cell (LBL) epitopes of the NS3 protein.
(DOCX)

S3 Table. Linear B cell (LBL) epitopes of the NS5B protein.
(DOCX)

S4 Table. Helper T Lymphocyte (HTL) epitopes of the NS5B protein.
(DOCX)

S5 Table. Helper T Lymphocyte (HTL) epitopes of the NS3 protein.
(DOCX)

S6 Table. Helper T Lymphocyte (HTL) epitopes of the P7 protein.
(DOCX)

S7 Table. Cytotoxic T Lymphocyte (CTL) epitopes of the P7 protein.
(DOCX)

S8 Table. Cytotoxic T Lymphocyte (CTL) epitopes of the NS3 protein.
(DOCX)

S9 Table. Cytotoxic T Lymphocyte (CTL) epitopes of the NS5B protein.
(DOCX)

S1 Fig. Prediction of the secondary structure of the construct 1 (A) and construct 2 (B) vaccines. The predicted results showed that among 686 amino acids in the construct 1, 268 (39.07%), 135 (19.68%), 66 (9.62%) and 217 (31.63%) amino acids are involved in α -helix, extended strand, beta turn, and random coil, respectively. Our predicted outputs revealed that among 607 amino acids in the construct 2, 205 (33.77%), 132 (21.75%), 63 (10.38%) and 207 (34.10%) amino acids are involved in α -helix, extended strand, beta turn, and random coil, respectively.
(DOCX)

S2 Fig. Linear (A and C) and Discontinuous (B and D) B-cell epitopes of the construct 1 (A and B) and construct 2 (C and D) vaccines (colored spheres).
(DOCX)

S3 Fig. The 3D view of the molecular docking conformations. The interface residues between two proteins TLRs (orange cartoon) and adjuvants (magenta cartoon) residues (orange and magenta sticks) are labeled. Hydrogen bonds and hydrophobic contacts are presented as green dashed line and arc with spokes radiating, respectively. A and B indicate TLR4-50S ribosomal protein L7/L12 and TLR3-human β -defensin 2 complexes, respectively.
(DOCX)

S4 Fig. A and B indicate TLR4-construct 1 and TLR3-construct 2 complexes, respectively. TLRs and constructs are depicted as brown and blue cartoons respectively.
(DOCX)

S1 Data. Multiple alignment of the NS3 protein sequences in HCV strains.
(PDF)

S2 Data. Multiple alignment of the P7 protein sequences in HCV strains.
(PDF)

S3 Data. Multiple alignment of the NS5B protein sequences in HCV strains.
(PDF)

Acknowledgments

This work was supported by the Iran National Science Foundation.

Author Contributions

Conceptualization: Esmaeil Behmard, Akbar Farjadfar, Ebrahim Barzegari, Amin Kouhpayeh.

Data curation: Esmaeil Behmard, Sohrab Najafipour, Abdolmajid Ghasemian, Parviz Abdolmaleki.

Formal analysis: Esmaeil Behmard.

Funding acquisition: Hussein T. Abdulabbas, Saade Abdalkareem Jasim, Ebrahim Barzegari.

Investigation: Esmaeil Behmard, Ebrahim Barzegari.

Methodology: Esmaeil Behmard, Ebrahim Barzegari.

Project administration: Sohrab Najafipour, Ebrahim Barzegari.

Resources: Abdolmajid Ghasemian, Parviz Abdolmaleki.

Software: Abdolmajid Ghasemian.

Supervision: Sohrab Najafipour, Ebrahim Barzegari.

Validation: Abdolmajid Ghasemian, Parviz Abdolmaleki.

Visualization: Abdolmajid Ghasemian.

Writing – original draft: Abdolmajid Ghasemian.

Writing – review & editing: Hussein T. Abdulabbas, Saade Abdalkareem Jasim, Abdolmajid Ghasemian, Akbar Farjadfar, Amin Kouhpayeh.

References

1. Lavanchy D. The global burden of hepatitis C. *Liver international*. 2009; 29:74–81. <https://doi.org/10.1111/j.1478-3231.2008.01934.x> PMID: 19207969
2. Drazan K. Molecular biology of hepatitis C infection. *Liver transplantation*. 2000; 6(4):396–406. <https://doi.org/10.1053/jlts.2000.6449> PMID: 10915159
3. Wilkins T, Malcolm JK, Raina D, Schade RR. Hepatitis C: diagnosis and treatment. *American family physician*. 2010; 81(11):1351–7. PMID: 20521755
4. Chen SL, Morgan TR. The natural history of hepatitis C virus (HCV) infection. *International journal of medical sciences*. 2006; 3(2):47. <https://doi.org/10.7150/ijms.3.47> PMID: 16614742
5. Sarrazin C, Hézode C, Zeuzem S, Pawlotsky JM. Antiviral strategies in hepatitis C virus infection. *Journal of hepatology*. 2012; 56:S88–100. [https://doi.org/10.1016/S0168-8278\(12\)60010-5](https://doi.org/10.1016/S0168-8278(12)60010-5) PMID: 22300469
6. Halfon P, Locarnini S. Hepatitis C virus resistance to protease inhibitors. *Journal of hepatology*. 2011; 55(1):192–206. <https://doi.org/10.1016/j.jhep.2011.01.011> PMID: 21284949
7. Penin F, Dubuisson J, Rey FA, Moradpour D, Pawlotsky JM. Structural biology of hepatitis C virus. *Hepatology*. 2004; 39(1):5–19. <https://doi.org/10.1002/hep.20032> PMID: 14752815
8. Dubuisson J. Hepatitis C virus proteins. *World journal of gastroenterology: WJG*. 2007; 13(17):2406.
9. Huang XJ, Lü X, Lei YF, Yang J, Yao M, Lan HY, et al. Cellular immunogenicity of a multi-epitope peptide vaccine candidate based on hepatitis C virus NS5A, NS4B and core proteins in HHD-2 mice. *Journal of virological methods*. 2013; 189(1):47–52. <https://doi.org/10.1016/j.jviromet.2013.01.003> PMID: 23333413
10. Kuhs KA, Ginsberg AA, Yan J, Wiseman RW, Khan AS, Sardesai NY, et al. Hepatitis C virus NS3/NS4A DNA vaccine induces multi-epitope T cell responses in rhesus macaques mimicking human immune responses. *Molecular Therapy*. 2012; 20(3):669–78.

11. Wang F, He XW, Jiang L, Ren D, He Y, Li DA, et al. Enhanced immunogenicity of microencapsulated multiepitope DNA vaccine encoding T and B cell epitopes of foot-and-mouth disease virus in mice. *Vaccine*. 2006; 24(12):2017–26. <https://doi.org/10.1016/j.vaccine.2005.11.042> PMID: 16414158
12. Tine JA, Firat H, Payne A, Russo G, Davis SW, Tartaglia J, et al. Enhanced multiepitope-based vaccines elicit CD8⁺ cytotoxic T cells against both immunodominant and cryptic epitopes. *Vaccine*. 2005; 23(8):1085–91. <https://doi.org/10.1016/j.vaccine.2003.01.001> PMID: 15620483
13. Liu Z, Behloul N, Baha S, Wei W, Shi R, Meng J. Design and immunogenicity analysis of the combined vaccine against zoonotic hepatitis E and foot-and-mouth disease. *Vaccine*. 2019; 37(46):6922–30. <https://doi.org/10.1016/j.vaccine.2019.09.036> PMID: 31604580
14. Verma S, Sugadev R, Kumar A, Chandna S, Ganju L, Bansal A. Multi-epitope DnaK peptide vaccine against *S. Typhi*: an in silico approach. *Vaccine*. 2018; 36(28):4014–22. <https://doi.org/10.1016/j.vaccine.2018.05.106> PMID: 29861180
15. Pandey RK, Prajapati VK. Exploring sand fly salivary proteins to design multiepitope subunit vaccine to fight against visceral leishmaniasis. *Journal of cellular biochemistry*. 2019; 120(2):1141–55.
16. Kar PP, Srivastava A. Immuno-informatics analysis to identify novel vaccine candidates and design of a multi-epitope based vaccine candidate against *Theileria* parasites. *Frontiers in immunology*. 2018; 9:2213. <https://doi.org/10.3389/fimmu.2018.02213> PMID: 30374343
17. Narula A, Pandey RK, Khatoon N, Mishra A, Prajapati VK. Excavating chikungunya genome to design B and T cell multi-epitope subunit vaccine using comprehensive immunoinformatics approach to control chikungunya infection. *Infection, Genetics and Evolution*. 2018; 61:4–15. <https://doi.org/10.1016/j.meegid.2018.03.007> PMID: 29535024
18. Chauhan V, Rungta T, Goyal K, Singh MP. Designing a multi-epitope based vaccine to combat Kaposi Sarcoma utilizing immunoinformatics approach. *Scientific reports*. 2019; 9(1):1–5.
19. Abdulla F, Adhikari UK, Uddin MK. Exploring T & B-cell epitopes and designing multi-epitope subunit vaccine targeting integration step of HIV-1 lifecycle using immunoinformatics approach. *Microbial pathogenesis*. 2019; 137:103791.
20. Srivastava PN, Jain R, Dubey SD, Bhatnagar S, Ahmad N. Prediction of epitope-based peptides for vaccine development from coat proteins GP2 and VP24 of Ebola virus using immunoinformatics. *International journal of peptide research and therapeutics*. 2016; 22(1):119–33.
21. Khalid H, Ashfaq UA. Exploring HCV genome to construct multi-epitope based subunit vaccine to battle HCV infection: Immunoinformatics based approach. *Journal of Biomedical Informatics*. 2020; 108:103498. <https://doi.org/10.1016/j.jbi.2020.103498> PMID: 32621883
22. Ikram A, Zaheer T, Awan FM, Obaid A, Naz A, Hanif R, et al. Exploring NS3/4A, NS5A and NS5B proteins to design conserved subunit multi-epitope vaccine against HCV utilizing immunoinformatics approaches. *Scientific reports*. 2018; 8(1):1–4.
23. Kar T, Narsaria U, Basak S, Deb D, Castiglione F, Mueller DM, et al. A candidate multi-epitope vaccine against SARS-CoV-2. *Scientific reports*. 2020; 10(1):1–24.
24. Oany AR, Emran AA, Jyoti TP. Design of an epitope-based peptide vaccine against spike protein of human coronavirus: an in silico approach. *Drug design, development and therapy*. 2014; 8:1139. <https://doi.org/10.2147/DDDT.S67861> PMID: 25187696
25. Morse ZJ, Horwitz MS. Innate viral receptor signaling determines type 1 diabetes onset. *Frontiers in endocrinology*. 2017; 8:249. <https://doi.org/10.3389/fendo.2017.00249> PMID: 29018409
26. Ahmad S, Shahid F, Tahir ul Qamar M, Rehman HU, Abbasi SW, Sajjad W, et al. Immuno-informatics analysis of PAKISTAN-based HCV subtype-3a for chimeric polypeptide vaccine design. *Vaccines*. 2021; 9(3):293. <https://doi.org/10.3390/vaccines9030293> PMID: 33801143
27. Sievers F, Higgins DG. Clustal Omega, accurate alignment of very large numbers of sequences. In *Multiple sequence alignment methods 2014* (pp. 105–116). Humana Press, Totowa, NJ.
28. Doytchinova IA, Flower DR. VaxiJen: a server for prediction of protective antigens, tumour antigens and subunit vaccines. *BMC bioinformatics*. 2007; 8(1):4. <https://doi.org/10.1186/1471-2105-8-4> PMID: 17207271
29. Gupta S, Kapoor P, Chaudhary K, Gautam A, Kumar R, Raghava GP. Peptide toxicity prediction. In *Computational Peptidology 2015* (pp. 143–157). Humana Press, New York, NY.
30. Dimitrov I, Flower DR, Doytchinova I. AllerTOP—a server for in silico prediction of allergens. In *BMC bioinformatics 2013*; 14, (6): p. S4. BioMed Central. <https://doi.org/10.1186/1471-2105-14-S6-S4> PMID: 23735058
31. Dhanda SK, Vir P, Raghava GP. Designing of interferon-gamma inducing MHC class-II binders. *Biology direct*. 2013; 8(1):30. <https://doi.org/10.1186/1745-6150-8-30> PMID: 24304645

32. Nagpal G, Usmani SS, Dhanda SK, Kaur H, Singh S, Sharma M, et al. Computer-aided designing of immunosuppressive peptides based on IL-10 inducing potential. *Scientific reports*. 2017; 7:42851. <https://doi.org/10.1038/srep42851> PMID: 28211521
33. Dhanda SK, Gupta S, Vir P, Raghava GP. Prediction of IL4 inducing peptides. *Clinical and Developmental Immunology*. 2013; 2013. <https://doi.org/10.1155/2013/263952> PMID: 24489573
34. Gasteiger E, Hoogland C, Gattiker A, Wilkins MR, Appel RD, Bairoch A. Protein identification and analysis tools on the Expasy server. In *The proteomics protocols handbook 2005* (pp. 571–607). Humana press.
35. Geourjon C, Deleage G. SOPMA: significant improvements in protein secondary structure prediction by consensus prediction from multiple alignments. *Bioinformatics*. 1995; 11(6):681–4. <https://doi.org/10.1093/bioinformatics/11.6.681> PMID: 8808585
36. Schwede T, Kopp J, Guex N, Peitsch MC. SWISS-MODEL: an automated protein homology-modeling server. *Nucleic acids research*. 2003; 31(13):3381–5. <https://doi.org/10.1093/nar/gkg520> PMID: 12824332
37. Wiederstein M, Sippl MJ. ProSA-web: interactive web service for the recognition of errors in three-dimensional structures of proteins. *Nucleic acids research*. 2007; 35(suppl_2):W407–10. <https://doi.org/10.1093/nar/gkm290> PMID: 17517781
38. Van Der Spoel D, Lindahl E, Hess B, Groenhof G, Mark AE, Berendsen HJ. GROMACS: fast, flexible, and free. *Journal of computational chemistry*. 2005; 26(16):1701–18. <https://doi.org/10.1002/jcc.20291> PMID: 16211538
39. Behmard E., Soleymani B., Najafi A., & Barzegari E. Immunoinformatic design of a COVID-19 subunit vaccine using entire structural immunogenic epitopes of SARS-CoV-2. *Scientific reports*. 2020; 10(1), 1–12.
40. Kozakov D, Hall DR, Xia B, Porter KA, Padhorna D, Yueh C, et al. The ClusPro web server for protein–protein docking. *Nature protocols*. 2017; 12(2):255. <https://doi.org/10.1038/nprot.2016.169> PMID: 28079879
41. DeLano WL. Pymol: An open-source molecular graphics tool. *CCP4 Newsletter on protein crystallography*. 2002; 40(1):82–92.
42. Wallace A. C., Laskowski R. A., & Thornton J. M. (1995). LIGPLOT: a program to generate schematic diagrams of protein-ligand interactions. *Protein engineering, design and selection*, 8(2), 127–134. <https://doi.org/10.1093/protein/8.2.127> PMID: 7630882
43. Krieger E, Joo K, Lee J, Lee J, Raman S, Thompson J, et al. Improving physical realism, stereochemistry, and side-chain accuracy in homology modeling: Four approaches that performed well in CASP8. *Proteins: Structure, Function, and Bioinformatics*. 2009; 77(S9):114–22.
44. Mora Lagares L, Minovski N, Caballero Alfonso AY, Benfenati E, Wellens S, Culot M, et al. Homology modeling of the human p-glycoprotein (Abcb1) and insights into ligand binding through molecular docking studies. *International journal of molecular sciences*. 2020; 21(11):4058.
45. Genheden S., & Ryde U. (2015). The MM/PBSA and MM/GBSA methods to estimate ligand-binding affinities. *Expert opinion on drug discovery*, 10(5), 449–461. <https://doi.org/10.1517/17460441.2015.1032936> PMID: 25835573
46. Dikhit M. R., Vijayamahantesh, Kumar A., Amit A., Dehury B., Nathsharma Y. P., & Das P. (2018). Mining the proteome of *Leishmania donovani* for the development of novel MHC class I restricted epitope for the control of visceral leishmaniasis. *Journal of cellular biochemistry*, 119(1), 378–391. <https://doi.org/10.1002/jcb.26190> PMID: 28585770
47. Dikhit M. R., Das S., Mahantesh V., Kumar A., Singh A. K., Dehury B., et al. (2018). The potential HLA Class I-restricted epitopes derived from LeIF and TSA of *Leishmania donovani* evoke anti-leishmania CD8+ T lymphocyte response. *Scientific reports*, 8(1), 1–13.
48. Dikhit M. R., Kumar A., Das S., Dehury B., Rout A. K., Jamal F., et al (2017). Identification of potential MHC Class-II-restricted epitopes derived from *Leishmania donovani* antigens by reverse vaccinology and evaluation of their CD4+ T-cell responsiveness against visceral leishmaniasis. *Frontiers in immunology*, 8, 1763. <https://doi.org/10.3389/fimmu.2017.01763> PMID: 29312304
49. Sabet LP, Taheri T, Memarnejadian A, Azad TM, Asgari F, Rahimnia R, et al. Immunogenicity of multi-epitope DNA and peptide vaccine candidates based on core, E2, NS3 and NS5B HCV epitopes in BALB/c mice. *Hepatitis monthly*. 2014; 14(10).